(19) Chiou, C. T.; Peters, L. J.; Freed, V. H. *Science (Washington, D.C.)* **1979**, *206*, 831–832.
(20) Karickhoff, S. W.; Brown, D. S.; Scott, T. A. *Water Res.* **1979**, *13*, 241–248.
(21) *Solubility of Inorganic and Organic Compounds*; Stephen, H., Stephen, T., Eds.; Macmillan: New York, 1963.

Received for review March 30, 1987. Revised manuscript received December 14, 1987. Accepted February 1, 1988. This research was supported by the U.S. Environmental Protection Agency under Cooperative Agreement CR-811743-01-0 with the R. S. Kerr Environmental Research Laboratory, Ada, OK. Although the research described in this paper has been funded wholly or in part by the U.S. Environmental Protection Agency through Assistance Agreement CR-811743-01-0 to the University of Maryland, it has not been subjected to Agency review and therefore does not necessarily reflect the views of the Agency, and no official endorsement should be inferred.

Application of the Precipitation–Charge Neutralization Model of Coagulation

Steven K. Dentel

Department of Civil Engineering, University of Delaware, Newark, Delaware 19716

■ A quantitative model is considered that develops predictions of suspension stability on the basis of electrokinetic characteristics of colloidal material prior to and following coagulation. The model is applied in this paper to coagulation with aluminum sulfate and other aluminum salts. The effect of increasing particle surface area on coagulation is first modeled for a system containing particulate silica, but of varying size and concentration. Experimental results show a correlation of turbidity removal to attainment of near neutral ζ potential in "zone 2" coagulation, and the calibrated model successfully predicts this zone. The model is then used to describe the coagulation of waters containing humic substances by considering them as small colloids with a substantial contribution to surface area in the system. Finally, it is shown that the model can be employed to describe the performance of polyaluminum coagulants as well.

Introduction

Coagulation with aluminum or iron salts, though one of the most common processes in water treatment, has long been understood only in qualitative terms. The two mechanisms invoked (*1*) to explain the observed phenomena have usually been (1) adsorption of soluble, positively charged metal hydroxide species, either monomeric or polymeric in nature, leading to charge neutralization or charge reversal of negatively charged colloidal material and (2) at much higher doses of coagulant, the formation of metal hydroxide precipitate in sufficient quantities to induce "sweep floc", which enmeshes and removes the original colloidal matter. Though these mechanisms have been in the literature for decades, there has been little success at developing quantitative models that utilize them toward practical application.

At the same time, it has become more common to map data from coagulation experiments onto axes of pH vs the negative log of molar coagulant dose, the latter quantity being expressed, for example, as p[Al] or p[Fe]. Such diagrams are known as stability domains in the colloidal science literature and more recently have been termed coagulation diagrams (*1*). They may be generated by a variety of procedures such as jar tests, electrophoresis methods, or smaller volume experiments. As long as the pH and amount of added coagulant are known, a sufficient amount of data then enables lines of equal degree of destabilization to be placed on the coagulation diagram. "Degree of destabilization" may be equated with such measured quantities as supernatant turbidity, absorbance, or electrophoretic mobility. Amirtharajah and co-workers (*1*, *2*) have shown that, for a given coagulant, experimental results tend to collapse into common regions on such diagrams, exemplified in Figure 1 by their diagram for coagulation with aluminum salts. These regions are then postulated to correspond with zones of coagulation due to the two mechanisms described above or to areas where neither means of destabilization has been manifested.

Unfortunately, these zones are not uniformly observed to fall into similar areas on such diagrams when a greater range of suspension types and coagulant forms are considered. As noted by Johnson and Amirtharajah (*2*) and Knocke (*3*), colloidal surface area and surface characteristics, as well as solution chemistry, may affect the location of these zones. For example, Figure 2 shows results for the alum coagulation of Norwegian surface waters reported by Vik et al. (*4*); these authors believed that their destabilization regimes did not correspond to those given by Amirtharajah and Mills due to the high concentration of humic substances in their waters. Laboratory studies by Dempsey et al. (*5*, *6*) and Edwards and Amirtharajah (*7*) in which controlled amounts of humic materials were coagulated have in fact demonstrated that coagulant demand is strongly dependent on humic concentration. Figure 3 shows the stability domain for a system containing both kaolinite and fulvic acid from Dempsey et al. (*6*) for which the optimum alum dose is generally intermediate to those indicated in Figures 1 and 2. Thus, it is not possible to create a generalized coagulation diagram that will designate appropriate coagulant doses for all waters, particularly those containing humic substances. Clearly, other variables must be taken into account if such systems are to be properly described.

Recently developed coagulation models (*8*, *9*) may enable such difficulties to be resolved. These quantitative models differ somewhat from the two mechanisms cited above in their means of explaining destabilization phenomena. They postulate that, under many conditions, the neutralization and reversal of colloid charge are caused by precipitation of positively charged metal hydroxide. The precise mechanism may be an initial adsorption or precipitation onto the colloidal surface, with this incipient solid phase then serving as a nucleation site for further precipitation. It is also possible that precipitation occurs in solution with rapid deposition onto the colloidal surfaces; this may be a less effective way of obscuring the original particle surface characteristics (*10*).

In this paper it is demonstrated that such models can be used to describe the coagulation of waters containing humic substances. The effect of increasing particle surface area on coagulation is first modeled for a system containing only larger particles, but of varying size and concentration. Humic substances may be considered either as soluble

0013-936X/88/0922-0825$01.50/0

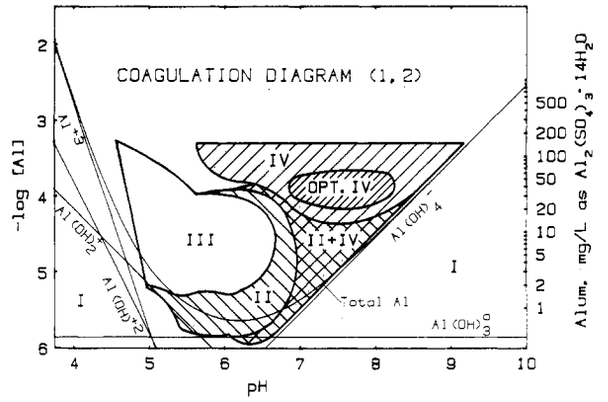

Figure 1. Alum coagulation diagram according to Amirtharajah and Mills (*1*) and Johnson and Amirtharajah (*2*). Indicated zones are as follows: I, stable suspension; II, adsorption destabilization; III, restabilization; IV, sweep coagulation, with optimum sweep zone also shown. Equilibrium concentrations of monomeric and total soluble aluminum at the solubility limit are also shown as calculated from Table I constants.

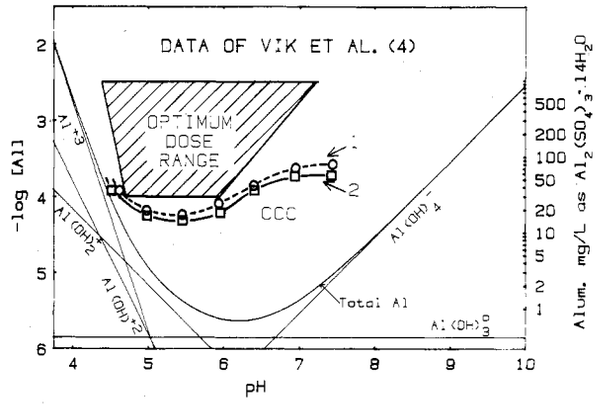

Figure 2. Alum coagulation results for Norwegian lakes investigated by Vik et al. (*4*). Curves indicate critical coagulation concentration (CCC) for Lake Hellerudmyra (1) and Lake Tjernsmotjern (2); shaded area shows the dose and pH range of optimal removal.

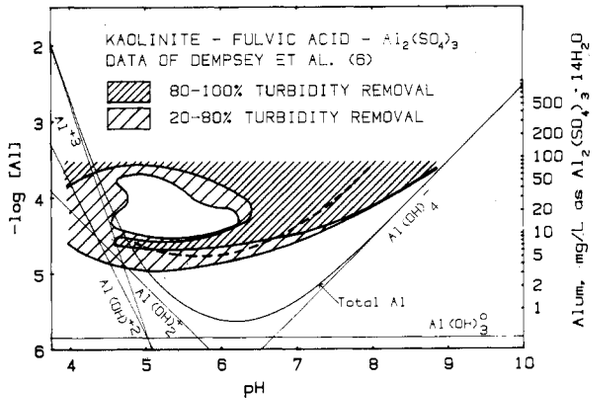

Figure 3. Alum coagulation results of Dempsey et al. (*5*) for a synthetic water prepared with 62.5 mg/L kaolinite and 0.85 mg/L fulvic acid (as TOC). Zones of greater than 80% and from 20 to 80% turbidity removal are indicated by shaded areas. Alum doses resulting in an EM of zero are shown by the dashed line.

macromolecules or as small colloids (*11*); the latter is assumed here, such that the coagulation of humics may be modeled by accounting for their substantial contribution to surface area in the system. Finally, it is shown that the same model can also be employed to describe the performance of polyaluminum coagulants.

The model considered in this paper develops predictions of suspension stability on the basis of electrokinetic

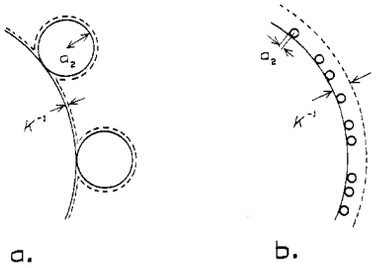

Figure 4. Schematic illustration of two possible conditions for aluminum hydroxide deposition onto particles: (a) the aluminum hydroxide species or particles are much larger than the dimensions of the EDL or (b) they are much smaller than the EDL.

characteristics of particulates prior to and following coagulation. The correlation of turbidity removal to attainment of near neutral ζ potential has been well-documented in the past for what is known as zone 2 coagulation (*12–15*), although the optimum coagulant dose may be at a ζ potential somewhat offset from zero due to other factors such as solvation and floc volume effects (*8*). A colloid titration technique (*15*) has also shown neutralization of colloidal charge to correspond with good removal of both color and turbidity. More recently, the success of streaming current detectors (SCDs) for on-line control of coagulant dosage further attests to the utility of electrokinetic parameters (*16*).

Model Development

The central assumption of the model is that the total charge of counterions in the diffuse layer about a coagulated particle is the sum of two component diffuse layer charges: that which counteracts charge on the original particle (including Stern or Helmholtz layer charges) and that which counteracts charge on the attached metal hydroxide contributed by the coagulant. Since each of these components is the product of a diffuse layer charge density and an area

$$\sigma_{1,2}(A_1 + A_2) = \sigma_1 A_1 + \sigma_2 A_2 \tag{1}$$

where σ = diffuse layer charge density, C/m^2, A = surface area, m^2/L, 1 = surface 1 (original particle), 2 = surface 2 (metal hydroxide), and 1,2 = overall assembly.

Values for σ_2 are assumed equal to the diffuse layer charge density of the metal hydroxide solid in the absence of other suspended material, but under the same solution conditions. A more convenient form of eq 1 is

$$\sigma_{1,2} = \frac{\sigma_1 C_1 + \sigma_2 C_2}{C_1 + C_2} \tag{2}$$

where

$$C_1 = C_2 A_1 / A_2 \tag{3}$$

and C_2 = moles per liter (bulk) of metal hydroxide deposited on surface 1.

If both the original particles and the metal hydroxide deposits are assumed spherical as shown in Figure 4, C_1 can be equated to other parameters. Of most interest is its relationship to the size of the deposited particles, since this provides insight into the mechanism of coagulation. Equations for C_1 are derived in the Appendix.

Equation 2 can be used in connection either with streaming current detectors, since SCD output is proportional to charge density (σ), or with colloid titration results, since the number of titratable groups is also related to charge density. Alternatively, the equation can be applied to ζ potential or electrophoretic mobility. The diffuse

Table I. Reactions and Equilibrium Constants for Hydrolysis of Al(III)

species	reaction	constant used[a]	ref
Al^{3+}	$Al(OH)_3(s) + 3H^+ \rightarrow Al^{3+} + 3H_2O$	$\log *K_{s0} = 9.15$	11[a]
$AlOH^{2+}$	$Al^{3+} + 1H_2O \rightarrow Al(OH)^{2+} + 1H^+$	$\log *\beta_1 = -4.97$	12, 13
$Al(OH)_2^+$	$Al^{3+} + 2H_2O \rightarrow Al(OH)_2^+ + 2H^+$	$\log *\beta_2 = -9.30$	12
$Al(OH)_3^0$	$Al^{3+} + 3H_2O \rightarrow Al(OH)_3^0 + 3H^+$	$\log *\beta_3 = -15.0$	12
$Al(OH)_4^-$	$Al^{3+} + 4H_2O \rightarrow Al(OH)_4^- + 4H^+$	$\log *\beta_4 = -21.7$	11

[a] Intermediate to given values.

layer charge density can be related to the outer plane (Stern or outer Helmholtz) electrical potential, ψ_d, by

$$\sigma = -\frac{2\epsilon kT\kappa}{ze}\sinh\left(\frac{ze\psi_d}{2kT}\right) \quad (4)$$

which, for $\psi_d < 25$ mV, reduces to a linear relationship between σ and ψ_d:

$$\sigma = -\epsilon\kappa\psi_d \quad (5)$$

where ϵ = bulk dielectric constant

$$\kappa = \text{inverse double-layer thickness} = \left(\frac{2000e^2N_AI}{\epsilon kT}\right)^{1/2} \quad (6)$$

z = ionic charge, e = unit electron charge, N_A = Avogadro's number, I = bulk solution ionic strength, k = Boltzmann constant, T = absolute temperature, and a_1 = radius of suspended particles. The equations are given in the SI system of units; the cgs system requires some changes in the constants involved.

It is then assumed that ψ_d is approximated by the measured ζ potential. (As a more exact alternative, a shear plane charge density σ_ζ could be defined as $\int_\chi^\infty \rho(z)dz$ where χ is the distance from the surface to the shear plane, ρ is the space charge density (C/m^3), and z is the distance normal to the surface. In eq 1, 2, 4, and 5, ζ would then be substituted for ψ_d and σ_ζ for σ.) It is further assumed that ζ is linearly related to the measured electrophoretic mobility (EM); e.g., for $\kappa a_1 > 100$, $\zeta = (EM)\mu/\epsilon$. Then, using eq 2 and 4 gives

$$(EM)_{1,2} = \frac{2\epsilon kT}{\mu ze}\sinh^{-1}\left[\frac{C_1\sinh\left(\frac{\mu ze(EM)_1}{2\epsilon kT}\right) + C_2\sinh\left(\frac{\mu ze(EM)_2}{2\epsilon kT}\right)}{C_1 + C_2}\right] \quad (7)$$

where μ is solution viscosity, and $2\epsilon kT/\mu ze = 3.75$ at 22 °C if EM is expressed as $\mu m\ s^{-1}\ (V/cm)^{-1}$. At EM values less than about 2 $\mu m\ s^{-1}\ (V/cm)^{-1}$, the sinh function approaches the value of its argument, and eq 7 is considerably simplified:

$$(EM)_{1,2} = \frac{(EM)_1C_1 + (EM)_2C_2}{C_1 + C_2} \quad (8)$$

For this equation, it need only be assumed that ψ_d is proportional to ζ. C_1 has units of concentration and is assumed constant for a given suspension and coagulant. It is initially used as an adjustable parameter since its component terms are unknown (see Appendix). C_2 is moles per liter of metal hydroxide in excess of the solubility limit, with the equilibrium and solubility constants in Table I (*17–19*). In other words

$$C_2 = C_{TOT} - \sum C_{N,M} \quad (9)$$

where C_{TOT} = total aluminum concentration (amount added as coagulant plus any original concentration) and $\sum C_{N,M}$ = sum of soluble aluminum species as aluminum. Thus, the model assumes that aluminum hydroxide deposition may be considered chiefly as a precipitation phenomenon. If adsorptive deposition were considered significant, appropriate additional expressions could also be incorporated.

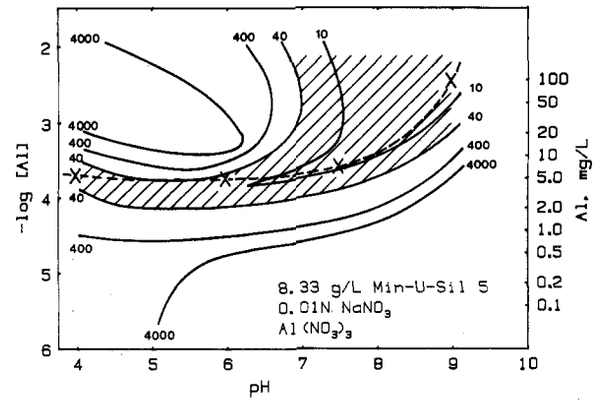

Figure 5. Stability plot for Min-U-Sil 5 at an original concentration of 8.33 g/L. Initial turbidity was 7650 nephelometric turbidity units (NTU). Lines of equal settled turbidity are shown with values given in NTU. The shaded area indicates residual turbidity less than 40 NTU, and the dashed line indicates conditions resulting in an EM of zero.

Using EM values for the original particles and the metal hydroxide precipitate at the same pH and ionic strength, EM values can then be predicted for the coagulated material with the above equations. Predictions can be placed on the same axes used for Figures 1–3 and compared with experimental data. This has already been done to validate the model for carefully controlled laboratory jar tests with very simple solid and solution phases (*20*). The present work was intended to extend the model's applicability to more complex systems, including coagulation of actual surface waters, to further confirm the model, and to possibly shed some light on coagulation mechanisms.

Experimental Methods

Silica suspensions consisted of Min-U-Sil 5 or Min-U-Sil 30 (PGS Corp., Pittsburgh, PA) in distilled, demineralized water. A concentration of 0.01 M $NaNO_3$ was included as an ionic strength buffer. Suspension volume was 500 mL. The coagulations were performed essentially as "jar tests" with a standard bench stirrer (Phipps and Bird, Richmond, VA), but the pH was held constant by NaOH during the rapid-mix stage. Coagulants employed were reagent-grade aluminum nitrate and aluminum sulfate, usually at concentrations of 0.1 M as Al. Rapid mix was for 3 min followed by flocculation at a velocity gradient of 30 s^{-1} for 20 min. Electrophoretic mobility of the flocculated particles was measured during this period; supernatant turbidity was determined following 30 min of settling. Further details concerning the procedure have been published elsewhere (*20*). Surface areas of Min-U-Sil samples were determined by conventional Brunauer–Emmett–Teller (BET) N_2 analysis.

Results

Silica Suspensions. Results for the jar tests using Min-U-Sil were utilized to develop stability domain plots

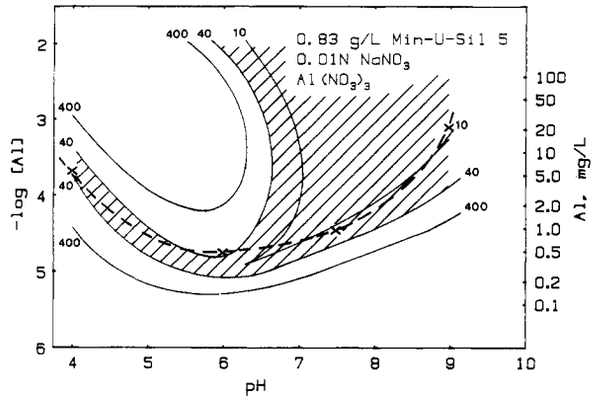

Figure 6. Stability plot for Min-U-Sil 5 at an original concentration of 0.83 g/L. Initial turbidity was 750 NTU. Lines of equal settled turbidity and zero EM are indicated as in Figure 5.

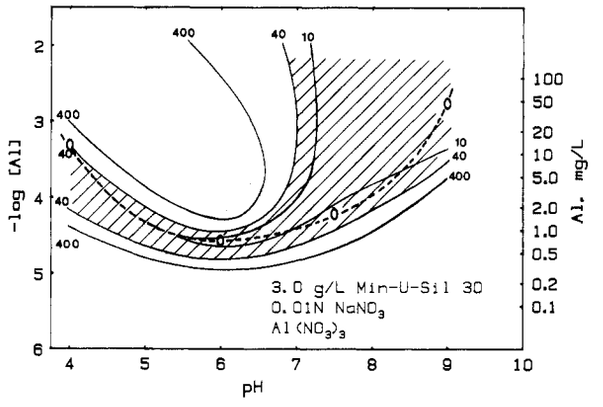

Figure 7. Stability plot for Min-U-Sil 30 at an original concentration of 3.0 g/L. Initial turbidity was 1350 NTU. Lines of equal settled turbidity and zero EM are indicated as in Figure 5.

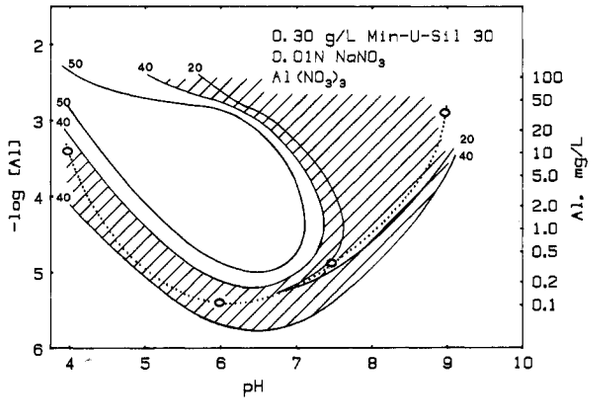

Figure 8. Stability plot for Min-U-Sil 30 at an original concentration of 0.30 g/L. Initial turbidity was 95 NTU. Lines of equal settled turbidity and zero EM are indicated as in Figure 5.

as previously described, with residual turbidity as the stability criterion. Figures 5 and 6 show the resulting graphs for Min-U-Sil 5 at respective concentrations of 8.33 and 0.83 g/L, and Figures 7 and 8 show those for Min-U-Sil 30 suspensions at original concentrations of 3.0 and 0.30 g/L. The dashed line in each of the four figures shows the conditions leading to an EM of zero, clearly indicating the correspondence between charge neutralization and particle destabilization at low doses. At higher doses, the effect of increased floc volume is to widen the EM range in which good flocculation occurs. Figure 9 combines the zero EM lines for all of the Min-U-Sil suspensions.

Model results for the same systems are given in Figure 10. The dashed lines, which show predicted aluminum

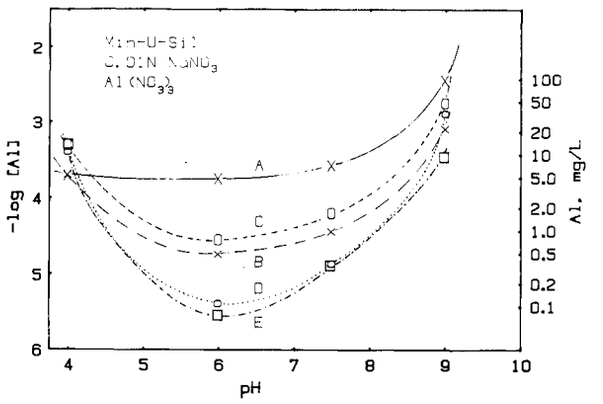

Figure 9. EM isopleths on the same axes used for previous figures. These lines show the pH and aluminum levels required to attain an EM of zero for all four silica suspensions. (A) 8.33 mg/L Min-U-Sil 5; (B) 0.83 mg/L Min-U-Sil 5; (C) 3.0 mg/L Min-U-Sil 30; (D) 0.30 mg/L Min-U-Sil 30; (E) 0.30 mg/L Min-U-Sil 30 coagulated with alum instead of aluminum nitrate.

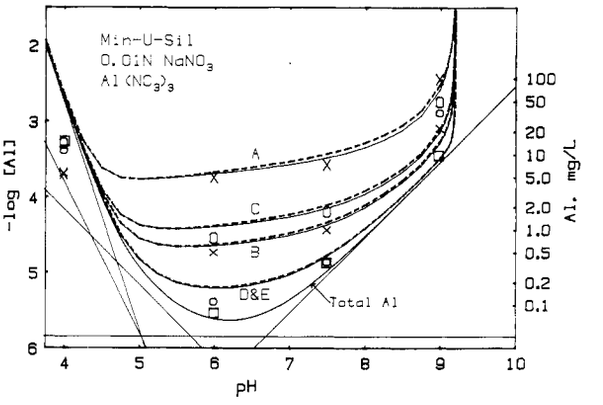

Figure 10. Model results for the silica suspensions. Dashed lines show predicted aluminum doses to produce zero EM by using eq 7. Solid lines are using the eq 8 approximation. (A) 0.83 mg/L Min-U-Sil 5; (B) 8.33 mg/L Min-U-Sil 5; (C) 0.30 mg/L Min-U-Sil 30; (D and E) 3.0 mg/L Min-U-Sil 30. The solubility limit for aluminum hydroxide precipitate is also shown.

doses to produce zero EM, were generated as follows. The solubility limit for aluminum hydroxide precipitate was first determined by using the species equilibria from Table I; this solubility limit is also shown in Figure 10. This amount of aluminum was then subtracted from the total amount added to give C_2 (eq 9). EM vs pH behavior for Min-U-Sil and aluminum hydroxide alone were determined previously (*20*, *21*), and the same characteristics were used as inputs for the present computations. Equation 7 was then used with C_1 initially unknown. A subjective best fit value for C_1 was determined for one suspension and held constant over all pH values; the values for C_1 to be used for other Min-U-Sil concentrations were then determined by the proportionality with measured surface areas required by eq 3. Table II provides the measured BET surface areas, corresponding surface area concentrations, and resulting C_1 values for the four systems. It can be seen that the agreement with EM measurements is good except at low pH, where adsorption of soluble aluminum hydroxide species may account for the discrepancies. Existence of the $Al(OH)_3^0$ species has also been questioned (*19*), and its elimination would improve the agreement.

Figure 10 also compares the model results of eq 7 with those using the approximation of eq 8 (solid lines). The hyperbolic sine function can evidently be dropped with little loss of accuracy.

Figure 11 shows the stability domain for 0.30 g/L Min-U-Sil 30 with aluminum sulfate rather than aluminum

Table II. Characteristics of Modeled Suspensions[a]

suspension type	BET surface area, m^2/g	A_1, m^2/L	κ^{-1}, nm	C_1 from model, M	a_2 by eq A3a, nm ($a_2 > \kappa^{-1}$)	a_2 by eq A3b, nm ($a_2 < \kappa^{-1}$)
Min-U-Sil 5, 8.33 g/L, I = 0.01 M	4.52	37.5	3.0	1.75×10^{-4}	1.23	0.31
Min-U-Sil 5, 0.83 g/L, I = 0.01 M	4.52	3.75	3.0	1.75×10^{-5}	1.23	0.31
Min-U-Sil 30, 3.0 g/L, I = 0.01 M	2.35	7.06	3.0	3.28×10^{-5}	1.23	0.31
Min-U-Sil 30, 0.30 g/L, I = 0.01 M	2.35	0.71	3.0	3.28×10^{-6}	1.23	0.31
Ludox AM, 2.0 g/L, I = ?	210	420	?	1.0×10^{-3}	0.63	0.16
zein, 0.10 g/L, I = 0.002 M	2.82	0.28	6.8	1.30×10^{-5}	12.3	3.07
cellulose, 0.10 g/L, I = 0.002 M	2.51	0.25	6.8	1.30×10^{-5}	13.8	3.44
fulvic acid, 3.5 mg/L TOC, I = ?	8000[b]	28[c]	?	3.0×10^{-5}	0.28	0.07

[a] Zein and cellulose from ref 20; Ludox AM from ref 21; fulvic acid from ref 5, 23. [b] Estimated values in m^2/g of TOC. [c] Estimated value.

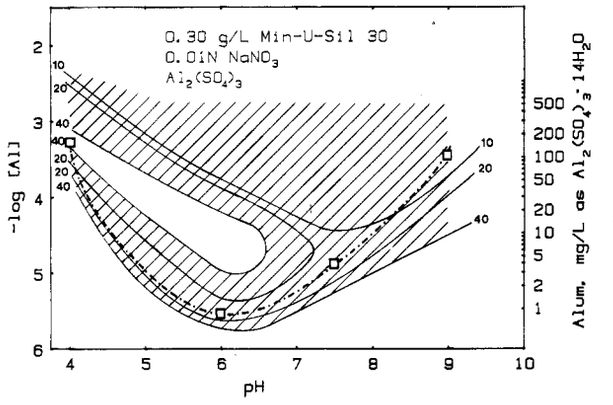

Figure 11. Stability plot for 0.30 g/L Min-U-Sil 30 using aluminum sulfate rather than aluminum nitrate as the coagulant. Lines of equal settled turbidity and zero EM are indicated as in Figure 5.

nitrate as the coagulant. Superimposed is the line of zero EM determined by measurement. Sulfate clearly mitigates the extent of charge reversal, evidently through its effect on the surface of the aluminum hydroxide as previously documented (*22*). However, the turbidity minima coinciding with charge neutralization are still successfully predicted by the model (Figures 10 and 11). Although the simplified model used here is primarily meant to describe charge neutralization, Letterman and Iyer (*9*) have shown that sulfate and floc volume effects can also be incorporated in such a model.

Humic Substances. The above results show that the effects of varying surface area on coagulation can be successfully modeled. If an appropriate surface area is assumed for a system containing humic substances, the model can be applied in this case as well. However, required model parameters are less accessible and must be inferred from other measurements on a well-characterized humic material.

Dempsey and O'Melia (*23*) presented titration data for several fulvic acid (FA) fractions and gave expressions describing the protonated and deprotonated fractions of sites according to these data. If the FA is considered as consisting of small, spherical colloids, then surface charge, surface potential, and ζ potential may be estimated vs pH for this material. Data were used for a sample which was resin extracted at pH 10 (denoted as FA 4) and characterized at ionic strength I = 0.01 M.

Equations and parameters used to estimate surface electrodouble-layer (EDL) characteristics for FA (and particles composed of agglomerated FA) are given in Table III. The equivalent radius of a single FA was found to be 1.4×10^{-7} cm, with a maximum possible charge density of 14 $\mu C/cm^2$. Calculated ζ potentials agreed well with values converted (empirically) from streaming current measurements made with an SCD (*16*). The calculated results were then used as input for the coagulation model.

Table III. Equations and Parameter Values Used To Characterize Fulvic Acid for Model (*23*, *24*)[a]

equation	parameter values
$\log K' = \log [\alpha_H/(1 - \alpha_H)] + pH$	$\log K^{int} = 1.91$
$\log K' = \log K^{int} + 0.869Wn(1 - \alpha_H)$	$0.869Wn = 3.56$ erg
$W = (3e^2/5\epsilon a_1)[1 + 0.6\kappa a_1 + 0.4(\kappa a_1)^2]$	$\kappa = 3.29 \times 10^6$ cm^{-1}
$m = \rho(4/3)\pi a_1^3$	$\rho = 1.05$ g/cm^3
$n = f_1 f_2 m N_A A_T$	$f_1 = 0.5$
	$f_2 = 0.5$
$\sigma_0 = nF(\alpha_H - 1)/4\pi a_1^2 N_A$	$A_T = 11.6$ mequiv/g of TOC
$\psi_0 = (2kT/e)\sinh^{-1}[\sigma_0(2kTN_A\epsilon I/\pi)^{1/2}]$	$T = 25$ °C
$\zeta = (4kT/e)\tanh^{-1}$ $[\exp(-\kappa\chi)\tanh(\psi_0 e/4kT)]$	$\chi = 2 \times 10^{-7}$ cm

[a] K' = apparent association constant; K^{int} = intrinsic association constant; α_H = protonated site fraction; W = electrostatic interaction term; n = sites per FA; m = mass per FA; ρ = density of hydrated FA in water; f_1 = weight fraction of FA in hydrated FA; f_2 = weight fraction of TOC per weight of dry FA; A_T = total sites per weight TOC; σ_0 = surface charge density; F = Faraday constant; ψ_0 = surface potential; χ = distance from surface to shear plane.

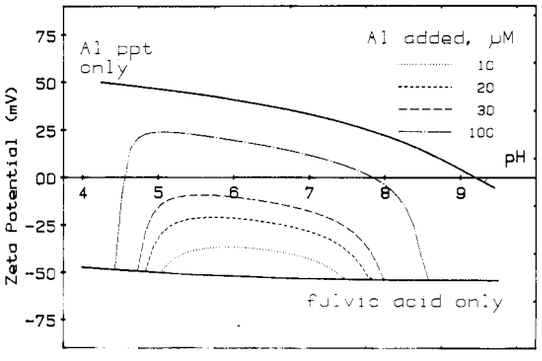

Figure 12. ζ potential vs pH for fulvic acid and aluminum hydroxide and model predictions for fulvic acid coagulated with 10, 20, 30, and 100 μM $AlCl_3$.

For example, Figure 12 shows ζ potential vs pH for the FA, for aluminum hydroxide precipitate, and for FA following various aluminum chloride additions. This graph shows how the model uses FA and $Al(OH)_3$ EM values as extrema, with the transition of coagulated-particle EM occurring first at intermediate pH levels where the solubility of aluminum hydroxide is the lowest.

The model was then used to predict the aluminum chloride doses producing integral values of EM. Dempsey et al. (*5*) coagulated the FA 4 fraction with aluminum chloride and presented stability domains in terms of FA removal (≥20%) by either settling or filtration. The data are compared to the model output in Figure 13 with a value of 3×10^{-5} M selected for C_1. The model's zone of charge neutralization then corresponds fairly well with the actual regime of destabilization. Agreement is least satisfactory in the lowest pH range, perhaps due to direct complexation

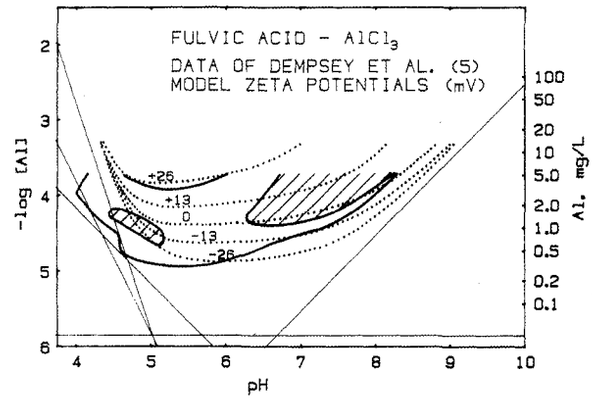

Figure 13. Comparison of model results with experimental data of Dempsey et al. (*5*) for coagulation of fulvic acid with aluminum chloride. Shaded areas indicate greater than 20% removal by settling; area inside dark lines indicates greater than 20% removal by filtering. Dotted lines indicate model results for constant values of ζ potential in mV.

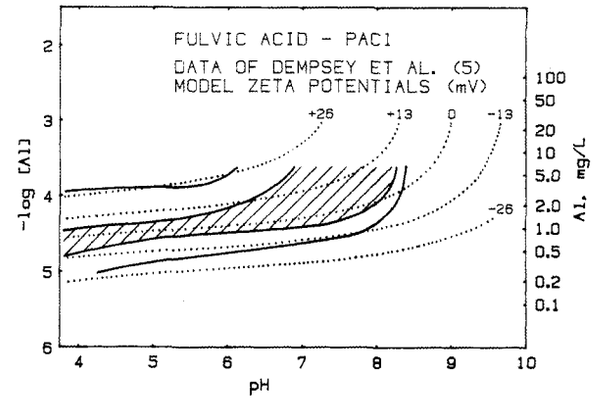

Figure 14. Comparison of model results with experimental data of Dempsey et al. (*5*) with polyaluminum chloride coagulant. Shaded areas indicate greater than 20% removal by settling; area inside dark lines indicates greater than 20% removal by filtering. Dotted lines indicate model results for constant values of ζ potential in mV.

of Al^{3+} with FA or to the particular values of equilibrium constants that were used.

Polyaluminum chloride. Dempsey et al. (*5*) also used a polyaluminum chloride (PACl) coagulant to destabilize this same FA fraction and showed that the stability domain differed substantially from that using aluminum chloride, particularly at pH extremes. PACl is produced by hydrolysis of aluminum chloride to create larger aluminum hydroxide species, with the most important of these believed (*19*) to consist of one central tetrahedral aluminum hydroxide surrounded by 12 octahedral aluminum hydroxides, commonly termed Al_{13}. This species is resistant to dissolution once formed (*5*). It may thus be hypothesized that the advantage of PACl at pH extremes stems from the circumvention of solubility limitations: in other words, the positively charged insoluble aluminum hydroxide species, which act as destabilizing agents, are preformed and do not depend on pH (or temperature) conditions within the water to be treated.

This concept may be incorporated into the coagulation model simply by replacing eq 9 with $C_2 = C_{TOT}$. If the same EM characteristics and C_1 value are employed as used for Figure 13, model results are as shown in Figure 14. Agreement with the experimental data of Dempsey et al. (*5*), also shown in Figure 14, is again quite good.

Discussion

The data shown in Figures 5–8 demonstrate the importance of surface area in determining coagulant demand. Although this dependency has been shown previously (e.g., ref 25), the results here suggest that a direct proportionality between coagulant demand and suspension surface area is not strictly correct; rather, it is the amount required in excess of the solubility limit, which is in proportion to surface area. This reduces to the former relationship in three cases: (1) in an intermediate pH range where the solubility of aluminum hydroxide species is very low; (2) in suspensions containing large surface area concentrations; (3) in the use of polyaluminum coagulants.

Surface area effects on coagulation are significant in water treatment, for example, during extreme fluctuations in raw water turbidity. In this case the concentration of particles larger than 1 μm may govern the coagulant demand, and the results using particulate silica are representative of this situation.

However, it has also been observed (*6*, *7*) that the concentration of color-causing organics may determine the required coagulant dosage. The model presented here successfully describes coagulation of humic materials and thereby explains their strong effect on the process: small concentrations of them provide large amounts of surface area to be neutralized. For example, the 3.5 mg/L FA system used in Figures 12–14 provides approximately the same surface area as 1700 mg/L of Min-U-Sil 5. Clearly, changes in humic content can radically change the surface area concentration in water regardless of its turbidity.

The model also provides an indication of how polyaluminum salts function. Apparently, their use eliminates the need to provide soluble aluminum species in order to attain the solubility limit of aluminum hydroxide. This would be a particular advantage at pH extremes where the solubility increases. In addition, kinetic limitations of forming polymers and/or precipitates of aluminum hydroxide—evidently of more concern at lower temperatures—are not of concern. Residual soluble aluminum concentrations might also be decreased, particularly if coagulation is performed at very low or high pH.

The model not only assumes that aluminum hydroxide precipitates onto particle surfaces but also enables the size of these destabilizing species to be estimated. Table II provides the values for A_1 and C_1 for systems considered in this and earlier papers, and the calculated values for a_2 using eq A3a ($a_2 > 1/\kappa$) and A3b ($a_2 < 1/\kappa$). The radius of monomeric aluminum hydroxide is about 0.327 nm (*14*); the radius of Al_{13} polymers has been reported as 1.3 nm, with further aggregation producing larger species (*26*). Although a considerable number of approximations are involved, comparison of these dimensions with calculated a_2 values in Table II suggests that monomeric aluminum hydroxide is the destabilizing species when coagulating silica. A similar value for a_2 has been calculated for the coagulation of TiO_2 with aluminum nitrate (*27*).

For the larger, organic particles of zein or cellulose, larger particles of aluminum hydroxide may arise via heterocoagulation before attaching to particles; on the other hand, the BET surface area measurements for such organic materials may be less reliable than for mineral substances. The surface area estimate for fulvic acid is also approximate, as are the assumptions of sphericity and monodispersity, so it is not clear whether either eq A3a or A3b is appropriate. Nonetheless, the results in Table II are realistic in magnitude and thus support the use of eq 1 and 2.

It is important to note that the model used in this paper is fairly simplified and does not describe a number of phenomena that can be significant factors in coagulation processes. These include the effects of (1) anions such as

sulfate that alter surface characteristics due to surface adsorption or double-layer compression, (2) increased particle volume and thus flocculation efficiency as a result of voluminous floc formation at high coagulant dosages, and (3) soluble species that may complex aluminum and alter its solubility. The model also does not consider the effects of mixing, though these could conceivably be incorporated into the computation of a_2.

Nonetheless, considering the simplicity of the model, its degree of success is remarkable. The above factors may be of negligible importance in many applications; for example, when chloride salts are used as coagulants, anion effects may be minimal. At moderate-coagulant doses, the alteration of particle surface charge is certainly more important than is the increase in floc volume fraction. Moreover, multiple jar tests at water treatment plants confirm the trends predicted by the model. Its use in a practical context has been discussed elsewhere (*28*).

Conclusions

Coagulation experiments varying pH, coagulant dose, particle size, and particle concentration demonstrate that, for destabilization by charge neutralization, the coagulant dose is related to aluminum hydroxide solubility, to charge density on the original particles, and to surface area of the original particles. For charge neutralization of silica particles, the aluminum added in excess of the aluminum hydroxide solubility limit is proportional to particle surface area. This is demonstrated by a simple but quantitative model for prediction of particle surface characteristics following coagulation. Also important in determining coagulant demand are the amounts of charge on the original colloid and on the aluminum hydroxide, which are model inputs. These may be provided either by direct measurement or by calculation.

Though the model neglects such aspects of coagulation as anion effects and the influence of floc volume on agglomeration, it still may be of practical use in some cases. As a conceptual tool, it provides explanations for the strong influence of subcolloidal humic substances on coagulant demand and for the mechanisms by which polyaluminum coagulants function.

Acknowledgments

The assistance of Todd Bober and Paul Ivans in conducting experimental work is gratefully acknowledged.

Appendix

If both the original particles and the metal hydroxide deposits are assumed spherical, C_1 can be equated to other parameters. Two different physical situations can be envisioned as illustrated in Figure 4: (a) the aluminum hydroxide species or particles are much larger than the dimensions of the electrodouble layer or (b) they are much smaller than it. Whether (a) or (b) applies should affect how these particles alter the electrokinetic properties of the overall assembly. The quantitative descriptions are similar for the two cases; suppose first that condition (a) applies. Also let N be the number of monomeric aluminum hydroxide molecules per deposited sphere. This number may be approximated by

$$N = a_2^3/a^3 \tag{A1}$$

where a_2 = radius of attached metal hydroxide (monomers, polymers, or particles) and a = radius of $Al(OH)_3(H_2O)_3$, 3.27 nm.

Then, since $A_2/(C_2/N)$ is the molar area of deposited spheres, combining with eq 3 and A1

$$A_2/C_2 = 4\pi a_2^2 N_A/N \tag{A2a}$$

and

$$C_1 = A_1 a_2/(4\pi a^3 N_A) \tag{A3a}$$

If it is also noted that

$$(4/3)\pi a^3 = w/(\rho_2 N_A) \tag{A4}$$

then a different expression for C_1 is

$$C_1 = \frac{A_1 \rho_2 a_2}{3w} \tag{A5a}$$

where ρ_2 = density of the metal hydroxide, and w = molecular weight of monomeric metal hydroxide.

The above expressions should be valid for $\kappa a_2 \gg 1$. If the aluminum hydroxide species are much smaller than the dimensions of the electrodouble layer (Figure 4b), then the area of these species that affects electrokinetic behavior of the overall particle may be approximated as their cross-sectional area rather than their surface area. In this case

$$A_2/C_2 = \pi a_2^2 N_A/N \tag{A2b}$$

and

$$C_1 = A_1 a_2/(\pi a^3 N_A) \tag{A3b}$$

or

$$C_1 = \frac{4A_1 \rho_2 a_2}{3w} \tag{A5b}$$

Registry No. PACl, 1327-41-9; SiO_2, 7631-86-9; Al_3NO_3, 13473-90-0; $Al_2(SO_4)_3$, 10043-01-3; cellulose, 9004-34-6.

Literature Cited

(1) Amirtharajah, A.; Mills, K. M. *J.—Am. Water Works Assoc.* **1982**, *74*, 210–216.
(2) Johnson, P. N.; Amirtharajah, A. *J.—Am. Water Works Assoc.* **1983**, *75*, 232–239.
(3) Knocke, W. R. *J. Environ. Eng. (N.Y.)* **1985**, *111*, 545.
(4) Vik, E. A.; Carlson, D. A.; Eikum, A. S.; Gjessing, E. T. *J.—Am. Water Works Assoc.* **1985**, *77(3)*, 58–66.
(5) Dempsey, B. A.; Ganho, R. M.; O'Melia, C. R. *J.—Am. Water Works Assoc.* **1984**, *76(3)*, 141–150.
(6) Dempsey, B. A.; Sheu, H.; Ahmed, T. M. T.; Mentink, J. *J.—Am. Water Works Assoc.* **1985**, *77(3)*, 74–80.
(7) Edwards, G. A.; Amirtharajah, A. *J.—Am. Water Works Assoc.* **1985**, *77(3)*, 50–57.
(8) Dentel, S. K. Ph.D. Dissertation, Cornell University, Ithaca, NY, 1984.
(9) Letterman, R. D.; Iyer, D. R. *Environ. Sci. Technol.* **1985**, *19*, 673–681.
(10) Krishnan, S. V.; Iwasaki, I. *Environ. Sci. Technol.* **1986**, *20*, 1224–1229.
(11) Liao, M. Y.; Randtke, S. J. *J.—Am. Water Works Assoc.* **1985**, *77(8)*, 77–88.
(12) Letterman, R. D.; Vanderbrook, S. G. *Water Res.* **1983**, *17*, 195–204.
(13) James, R. O.; Healy, T. W. *J. Colloid Interface Sci.* **1977**, *59*, 381–385.
(14) White, D. W. Ph.D. Dissertation, Clarkson College of Technology, Potsdam, NY, 1980.
(15) Kawamura, S.; Hanna, G. P., Jr.; Shumate, K. S. *J.—Am. Water Works Assoc.* **1967**, *59*, 1003–1013.
(16) Dentel, S. K.; Kingery, K. M. *An Evaluation of Streaming Current Detectors*; American Water Works Association Research Foundation: Denver, CO, 1988.
(17) Sillén, L. G.; Martell, A. E. *Spec. Publ.—Chem. Soc.* **1964**, *No. 17*; **1971**, *No. 25*.
(18) Stumm, W.; Morgan, J. J. *Aquatic Chemistry*, 2nd ed.; Wiley Interscience: New York, 1981.
(19) Baes, C. F., Jr.; Mesmer, R. E. *The Hydrolysis of Cations*; Wiley: New York, 1976.

(20) Dentel, S. K.; Gossett, J. M. *J.—Am. Water Works Assoc.* **1988**, *80*, 187–198.
(21) Matijevic, E.; Mangravite, F. J., Jr.; Cassell, E. A. *J. Colloid Interface Sci.* **1971**, *35*, 560–568.
(22) Letterman, R. D.; Vanderbrook, S. G.; Sricharoenchaikit, P. *J.—Am. Water Works Assoc.* **1982**, *74*, 44–51.
(23) Dempsey, B. A.; O'Melia, C. R. In *Aquatic and Terrestrial Humic Materials*; Christman, R. F., Gjessing, E. T., Eds.; Ann Arbor Science: Ann Arbor, MI, 1983; pp 239–273.
(24) Tanford, C. *Physical Chemistry of Macromolecules*; Wiley: New York, 1961.
(25) Stumm, W.; O'Melia, C. R. *J.—Am. Water Works Assoc.* **1968**, *60*, 514–525.
(26) Bottero, J. Y.; Tchoubar, D.; Cases, J. M.; Fiessinger, F. *J. Phys. Chem.* **1982**, *86*, 3667.
(27) Chern, J.-M. Master's Thesis, University of Delaware, Newark, DE, 1987.
(28) Dentel, S. K. In *Proceedings of the AWWA Seminar on Influence of Coagulation on the Selection, Operation, and Performance of Water Treatment Facilities*; American Water Works Association: Denver, CO, 1987; pp 49–88.

Received for review September 17, 1987. Accepted January 26, 1988. This study was funded by the University of Delaware Research Foundation and by National Science Foundation Grant ECE-8504898.